Synthesis, Biological Activities, DFT, and Molecular Docking Analysis of Two Sulfonamide Derivatives of 2(3H)-Benzoxazolone

Faouzi Guenadil[1], Hanene Nessaibia[2]* and Khadidja Otmane Rachedi[3]
[1]Laboratory of Organic and Medicinal Chemistry, Department of Chemistry, University of Chadli Bendjedid El Tarf-36000, Algeria
[2]Functional and Evolutionary Ecology" research laboratory, Department of Biology Sciences, Faculty of Natural and Life Sciences, Chadli Bendjedid University, El Tarf, Algeria.
[3]Faculty of Science and Technology, Department of Chemistry, Laboratory of Applied Organic Chemistry, Chadli Bendjedid University, El Tarf 36000, Algeria.
*Corresponding author (e-mail: h.nessaibia@univ-eltarf.dz)

Two sulfonamide derivatives of 2(3H)-benzoxazolone were synthesised using ultrasonic irradiation, by condensation of para-toluenesulfonyl chloride with 6-amino-2(3H)-benzoxazolone and 6-amino-3-methyl-2(3H)-benzoxazolone, in the presence of triethylamine and methylene chloride as solvent. This environmentally friendly synthesis method had short reaction times and gave excellent yields. Characterization of the products were performed using FT-IR, (^{1}H, ^{13}C NMR) and GC-MS. These compounds were screened for their antimicrobial activity. Compound M2 exhibited the strongest antibacterial activity against both Gram-positive and Gram-negative bacteria. Compound M2 exhibited the highest DPPH radical-scavenging activity, with an IC_{50} of 0.40 µg/mL. The molecular docking study against dihydropteroate synthase (PDB ID 3TZF) showed that both compounds exhibited favourable binding affinities and strong interactions with the enzyme. DFT analyses provided important insights into the chemical reactivity of the two compounds, including molecular electrostatic potential, Fukui indices, and global descriptors. Both compounds exhibited outstanding drug-like properties, with generally acceptable toxicity profiles.

Keywords: Biological activities, 2(3H)-benzoxazolone, Green synthesis, sulfonamide, DFT Calculation, Molecular docking

Received: September 2025; Accepted: February 2026

The emergence and spread of multidrug-resistant bacterial strains globally has weakened the effectiveness of antibiotics, one of the most significant medical achievements of the 20th century. Antibiotics have historically played a crucial role in combating bacterial infections and significantly reducing mortality rates worldwide [1]. With the rise of this resistance, treating many infections using traditional antibiotics has become more difficult, and sometimes impossible [2, 3]. Recent studies have demonstrated the essential role of oxidative stress in the development and spread of bacterial infections [4-7]. This situation underscores the urgent need to develop novel and innovative antimicrobial and antioxidant compounds. Pharmacological research strategies for the synthesis of bioactive compounds often focus on molecules widely used as therapeutic agents, such as the 2(3H)-benzoxazolone heterocycle, which plays a crucial role in various biological processes [8]. 2(3H)-benzoxazolone derivatives have attracted considerable attention due to their diverse biological activities including antioxidant [9, 10], anticancer, anti-ulcer [11], anti-HIV [12], antiviral [13], antibacterial, analgesic, and anti-inflammatory effects [14, 17]. Substitution at the 6-position of the benzoxazolone core crucially modulates biological activity, enabling the design of novel, efficient, and cost-effective synthetic pathways [15-17].

Recent years have seen ultrasound irradiation emerge as one of the most promising green chemistry techniques in organic synthesis. This method dramatically accelerates reactions, boosts yields, and reduces energy consumption through acoustic cavitation, where bubble formation and collapse enhance mass transfer and drive transformations under mild conditions [18-21].

Sulfonamides are a well-established class of synthetic drugs famous for their wide-ranging antibacterial, antifungal, anticancer, and antioxidant effects [22-27]. Adding sulfonamide groups to heterocyclic structures markedly improves their pharmacological profiles, increasing both potency and specificity [28, 29]. Given the potent therapeutic potential of both 2(3H)-benzoxazolone and sulfonamide structures, introduction of a sulfonamide group at the C-6 position of the 2(3H)-benzoxazolone nucleus is a logical and promising strategy for the design of new therapeutic agents. This molecular fusion is expected to enhance biological activity and expand the therapeutic applications of these compounds [30-32].

In this study, we report a novel, green, and efficient synthesis of two sulfonamide derivatives of 2(3H)-benzoxazolone (M1 and M2) using ultrasonic irradiation. The in vitro antimicrobial and antioxidant activities of these compounds were evaluated for the first time.

EXPERIMENTAL

Chemicals and Materials

Reaction progress was monitored by thin-layer chromatography (TLC) on silica gel 60 F254 plates (E. Merck, Darmstadt, Germany, ref. 5735) using a solvent mixture of ethyl acetate/cyclohexane (70:30). Melting points were measured using a Banc-Koffler apparatus. UV-Vis spectra of compounds M1 and M2 were recorded using a double-beam UV-Vis spectrophotometer, with dichloromethane as the reference solvent. The maximum absorption wavelengths (λ_{max}) were reported in nanometers (nm). NMR spectra were acquired using a Bruker spectrometer operating at 400 MHz for ^{1}H NMR and 101 MHz for ^{13}C NMR, with DMSO-d_6 as the solvent and tetramethylsilane (TMS) as the internal standard. Infrared spectra were recorded using a PerkinElmer 600 FTIR spectrometer. GC-MS analysis of the synthesized compounds was performed at the Technical Platform of Physico Chemical Analysis (PTAPC-CRAPC) in Laghouat, Algeria, using a SHIMADZU GCMS-QP2020 instrument.

General Procedure for the Synthesis of Compounds M1 and M2

In a 50 mL beaker, 1 mmol of 6-amino-2(3H)-benzoxazolone (0.150 g) or 6-amino-3-methyl-2(3H)-benzoxazolone (0.164 g) was dissolved in 20 mL of dichloromethane. 1.5 mmol of p-toluene sulfonyl chloride (0.280 g) was then added slowly at 0 °C in the presence of triethylamine (1.5 equivalents). The reaction mixture was subjected to ultrasonic irradiation for 5-10 minutes. It was subsequently washed with 20 mL of 0.1N of HCl, followed by 30 mL of water. The organic phase was then washed with saturated sodium bicarbonate solution, dried over anhydrous magnesium sulfate, filtered, and concentrated under reduced pressure. The crude product was recrystallized from ethanol to afford compounds M1 and M2.

Spectral Data of the Synthesized Compounds:

4-methyl-N-(3-methyl-2(3H)-benzoxazolon-6-yl) benzenesulfonamide (M1)

$C_{15}H_{14}N_2O_4S$; (Yellow powder), **yield** = 91 %, **Rf** = 0.25 (ethyl acetate/cyclohexane: 7/3), **M.p** =150-152 °C, **FTIR (KBr)**: ν (cm^{-1}) =3499, 2930, 1750, 1655, 1385, 1164. **^{1}H-NMR (DMSO-d6)**: δ (ppm) = 2.33 (s, 3H, CH3), 3.26 (s, 3H, CH3), 6.82 (s, 1H, 1Ar-H), 6.91 (dd, J_1 = 8.4 Hz, J = 2.1 Hz, 1H, 1Ar-H), 7.03 (d, J = 1.9 Hz, 1H, 1Ar-H), 7.31 (d, J = 8.02 Hz, 2H, 2Ar-H), 7.61 (d, J = 8.3 Hz, 2H, 2Ar-H), δ 9.93 (S, 1H, H-N-SO2). **^{13}C NMR (DMSO-d6)**: δ (ppm) = 21.34, 28.48, 109.46, 117.68, 127.22, 128.38, 129.25, 130.03, 133, 137.25, 142.45, 143.60, 154.4. **MS: m/z** [M^+] = 319.5. **λ max** = 300 (nm)

4-methyl-N-(2(3H)-benzoxazolon-6-yl) benzene sulfonamide (M2)

$C_{14}H_{12}N_2O_4S$; (Brown powder), **yield** = 78 %, **Rf** = 0.3 (ethyl acetate/cyclohexane: 7/3), **M.p** =190 °C, **FTIR (KBr)**: ν (cm^{-1}) = 3500, 3600, 2950, 1750, 1650, 1350, 1150. **^{1}H-NMR (DMSO-d6)**: δ (ppm) = 2.33 (s, 3H, CH3), 6.85 (dd, J = 8.3Hz, J = 2.3 Hz,1H, 1Ar-H), 6.92 (S, 1H, 1Ar-H), 7.0 (d, J = 1.9 Hz, 1H, 1Ar-H), 7.32 (d, J = 8.1 Hz, 2H, 2Ar-H), 7.61 (d, J = 8.3 Hz,2H, 2Ar-H), 9.98 (S, 1H, HN-SO2), 11.85 (s, 1H, N-H). **^{13}C NMR (DMSO-d6)**: δ (ppm) = 21.32, 110.24, 117.73, 126.04, 127.21, 127.81, 128.44, 130, 132.69, 137.26, 143.87, 154.79. **MS: m/z** [M^+] = 305.03. **λ max** = 360 (nm).

Biological Activities

Antibacterial Activity

The antibacterial activity of the synthesized compounds M1 and M2 was assessed using the agar well diffusion method as previously described, with minor modifications **[33, 34]**. The compounds were tested at concentrations of 1000 µg/mL, 500 µg/mL, and 250 µg/mL against three Gram-negative bacteria (*Escherichia coli, Salmonella Typhimurium, and Pseudomonas aeruginosa*) as well as three Gram-positive strains (*Staphylococcus aureus, Bacillus cereus, and Enterococcus faecalis*). Bacterial suspensions were standardized to 0.5 McFarland and innoculated into nutrient broth. Mueller-Hinton agar plates were swabbed with 0.1 mL of these suspensions. Wells of 6 mm diameter were created and loaded with 50 µL of each compound solution. Gentamicin (1000 µg/mL) served as the positive control, and DMSO as the negative control. Plates were incubated at 37 °C for 24 h, and inhibition zones (mm) were measured to determine the antibacterial efficacy of the compounds.

Antioxidant Activity

Antioxidant activity was evaluated using the DPPH radical scavenging assay, with minor modifications to established protocols, based on their capacity to neutralize the DPPH (2,2-diphenyl-1-picrylhydrazyl) radical [35]. Solutions of the compounds were prepared in DMSO at concentrations of 100, 200, 500, and 800 µg/mL, with ascorbic acid used as the positive control. Each sample was treated with 1 mL of 0.1 mM DPPH in methanol and incubated in the dark at room

temperature for 30 min. Absorbance was measured at 517 nm using a UV-Vis spectrophotometer, and the percentage of radical scavenging activity (%RSC) was calculated according to the standard formula:

$$\%RSC = 100 * [(A\ blank - A\ sample) / A\ blank]$$

where (A blank) and (A sample) are the DPPH solution absorbance without the sample and the DPPH solution absorbance with the sample, respectively. The IC_{50} values, representing the concentration required to scavenge 50 % of the DPPH radicals, were determined from the dose response curve. The results, including the radical scavenging activity percentage at each concentration, are presented along with the IC_{50} values for each compound.

Computational Studies

DFT Calculation

In this study, the properties of the two compounds M1/M2, were investigated using the DFT method with the 6-31G+(d,p) basis set and B3LYP functional. All computations were performed using Gaussian 16 software [36]. Following structural optimization, the optimized geometries were used to generate and analyze molecular electrostatic potential (MEP) maps, Fukui indices, and to calculate orbital energies. The HOMO and LUMO energies, their gap, and the global reactivity parameters were computed according to Koopmans' theorem [37].

Molecular Docking Study

The crystal structure of dihydropteroate synthase (DHPS, PDB ID: 3TZF) was obtained from the RCSB Protein Data Bank (http://www.pdb.org). The structures were prepared and their energies minimized using the Protein Preparation Wizard from the Schrödinger Suite prior to docking [38]. Grid files for the docking simulations were generated using Maestro 16.8's Glide Grid Generation tool, focusing on the ligands bound to DHPS. The scaling factor for van der Waals interactions of non-polar atoms was set to 0.8 to account for receptor flexibility, while all other parameters were kept at default values. For flexible docking, only the precision docking mode was employed. Docking results were visualized using Discovery Studio Visualizer.

Drug-Likeness and Toxicity Prediction

In silico drug-likeness analysis predicts whether a pharmacological compound possesses properties suitable for oral bioavailability. This evaluation is based on Lipinski's Rule of Five, a well-established criterion proposed by Lipinski et al [39]. Drug-likeness and toxicity predictions were performed to evaluate the pharmacokinetic and safety profiles of compounds M1 and M2. The drug-likeness assessment was carried out using the SwissADME tool (http://www.swissadme.ch/). The analysis focused on key properties, including oral bioavailability, gastrointestinal (GI) absorption, and blood-brain barrier (BBB) permeability. Additionally, toxicity predictions covering LD50, toxicity class, and organ-specific toxicities such as hepatotoxicity, carcinogenicity, immunotoxicity, mutagenicity, and cytotoxicity were conducted using the ProTox-II tool (http://tox.charite.de/protox_II) to determine the safety profile of the two compounds.

RESULTS AND DISCUSSION

Chemistry

The synthesis procedure was carried out under ultrasound irradiation, in the presence of triethylamine as a base catalyst, following previously reported methods [40-44]. The synthetic pathway leading to compounds M1 and M2 is illustrated in **Scheme 1**.

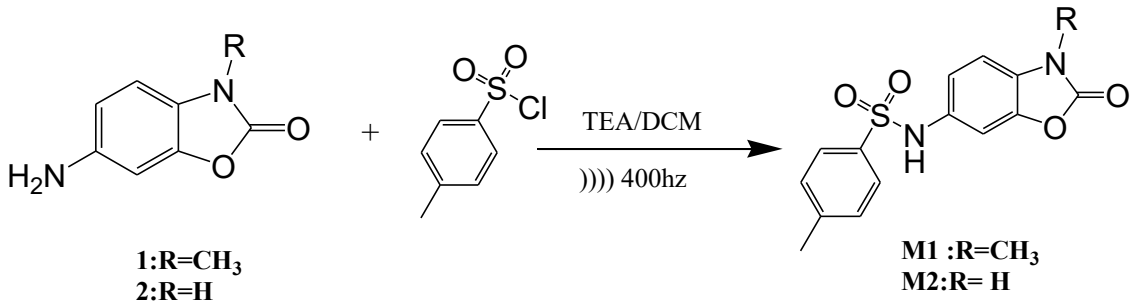

Scheme 1. Green synthesis of the two sulfonamide derivatives of 2(3H)-benzoxazolone, M1 and M2.

Table 1. Physicochemical properties of the synthesized compounds M1 and M2.

Product	R	Mp (°C)	Time	[b]Yield (%)
M1	CH_3	150-152	5	91
M2	H	190	10	78

Amine derivatives 1 and 2, used as starting materials, were prepared as previously reported in the literature [45-50]. These compounds were then subjected to a condensation reaction with a sulfonyl chloride derivative in the presence of triethylamine in dichloromethane under ultrasound irradiation. The final target compounds M1 and M2 were obtained with good yields achieved within a short reaction time (5-10 minutes) (**Table 1**).

Ultrasonic irradiation enhances organic reactions by generating acoustic cavitation in the reaction medium, which produces intense micro-agitation and significantly improves mass transfer between reactants and catalytic sites. These physical effects increase the effective contact area, thereby accelerating reaction rates and improving product yields. Additionally, ultrasonic treatment can disrupt solvation layers around reactant molecules, increasing their chemical reactivity and facilitating transformation under milder conditions. This strategy aligns with the principles of green chemistry, as it enables reactions to proceed at lower temperatures, shorter reaction times, and with reduced energy consumption compared to conventional methods [51-54]. The substantial gains in yield and the notable decrease in reaction times when compared to traditional thermal procedures demonstrate the crucial role of ultrasonic irradiation in our investigation [55]. The products were purified and characterized using UV-VIS, FT-IR, ^{1}H and ^{13}C NMR, and GC-MS analyses.

Antibacterial Activity

The antibacterial activity results, presented in **Figure 1**, demonstrate varying levels of efficacy, with inhibition zones ranging from 6 to 23 mm. Compound M2, at the highest concentration (1000 µg/mL), produced inhibition zones of 19 and 23 mm against *Escherichia coli* and *Salmonella Typhi*, respectively, comparable to gentamicin (20 mm for *E. coli* and 30 mm for *S. Typhi*), indicating strong antibacterial activity. In contrast, compound M1 showed moderate effects, with inhibition zones of 15 mm and 20 mm against the same strains. Neither compound was active against *Pseudomonas aeruginosa*, suggesting an intrinsic resistance of this strain to the tested derivatives. At lower concentrations, the activity of both compounds decreased markedly, with M2 retaining moderate inhibition at 500 µg/mL, whereas M1 exhibited only weak activity. Compound M2 also showed superior activity to M1 against all tested Gram-positive strains. At 1000 µg/mL, M2 produced inhibition zones of 11, 17, and 22 mm against *Staphylococcus aureus*, *Enterococcus faecalis*, and *Bacillus cereus*, respectively. Notably, its activity against *B. cereus* (22 mm) slightly exceeded that of gentamicin (20 mm), underscoring its potential as a potent antibacterial agent. In comparison, M1 displayed significant activity only against *B. cereus* (19 mm) and was inactive against *S. aureus* and *E. faecalis* at the same concentration. At 500 µg/mL, M2 maintained moderate inhibition (8-16 mm), whereas M1 was nearly inactive, and at 250 µg/mL, M2 had only a slight effect against *B. cereus* (6 mm). Overall, compound M2 exhibited higher antibacterial activity than M1 against both Gram-negative and Gram-positive strains, with particularly pronounced effects against *Bacillus cereus* and *Salmonella Typhi*. The larger inhibition zones observed for Gram-positive bacteria suggest that M2 may interact more effectively with their cellular components, possibly due to differences in cell wall permeability. Compared with the standard gentamicin, M2 showed comparable or even superior activity against certain strains, making it a promising candidate for further development as an antimicrobial agent. The observed dose-dependent activity also highlights the importance of compound concentration in achieving optimal antibacterial efficacy.

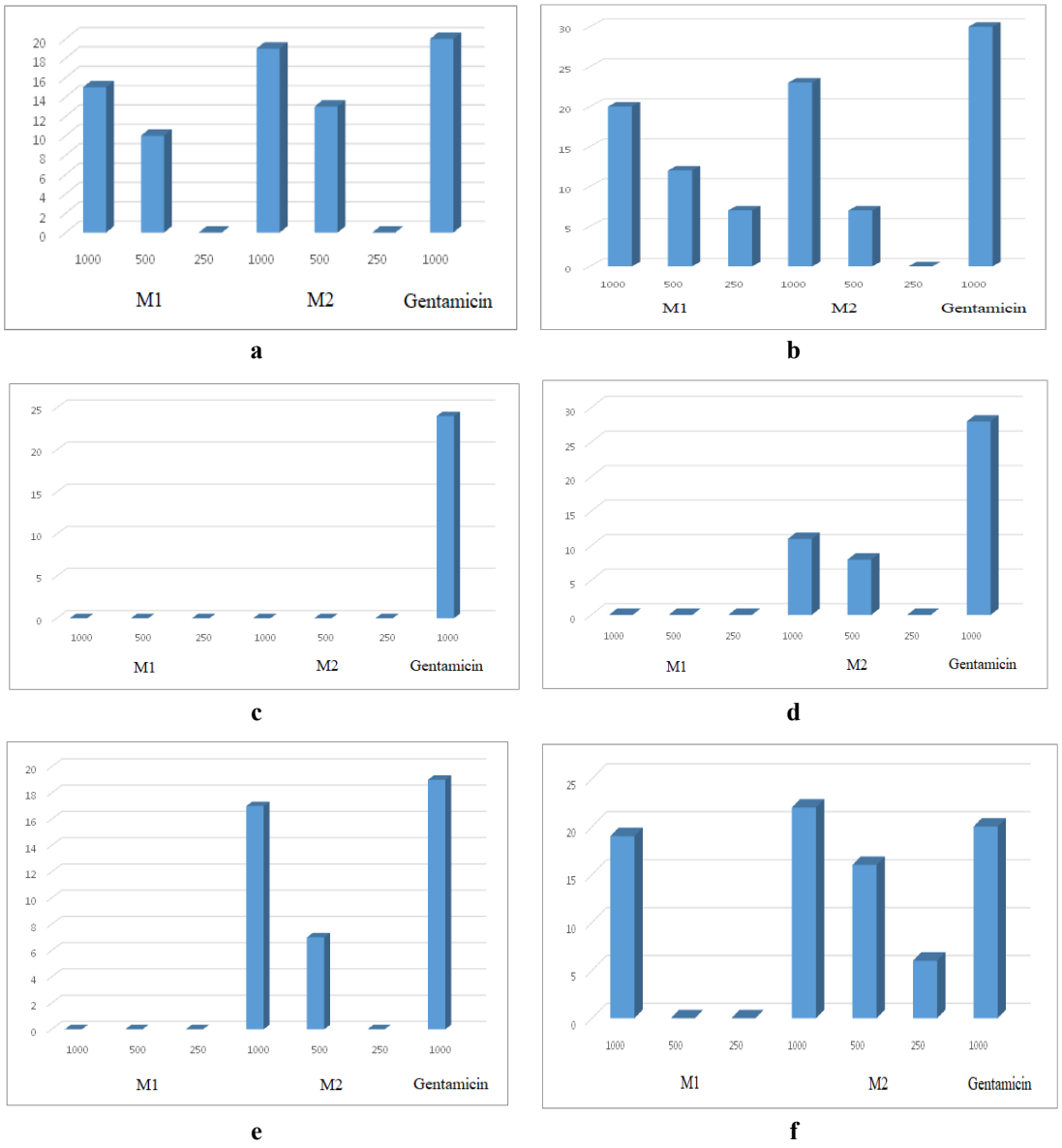

Figure 1. Antibacterial activity of the synthesized compounds M1 and M2 against (a) *Escherichia coli*, (b) *salmonella typhimurium*, (c) *pseudomonas aeruginosa* and the gram-positive strains (d) *staphylococcus aureus*, (e) *enterococcus faecalis*, and (f) *bacillus cereus*.

Antioxidant Activity

The antioxidant activity of compounds M1 and M2 was evaluated and compared with that of ascorbic acid, the reference standard (see **Table 3** and **Figure 2**). This assessment was based on the percentage of Radical Scavenging Capacity (RSC) and the IC_{50} value, which represents the concentration required to achieve 50 % radical scavenging, where lower IC_{50} values indicate stronger antioxidant activity [56-58]. Notably, a compound with an IC_{50}< 10 µg/mL is regarded as exhibiting potent antioxidant activity, meaning it is highly effective at neutralizing free radicals [59]. Compared to compound M1 (IC_{50} = 0.46 µg/mL), M2 showed a slightly lower IC_{50} (0.40 µg/mL) and a higher radical scavenging capacity (%RSC), indicating superior antioxidant activity. At the highest tested concentration (800 µg/mL), M2 reached 68.84 % RSC, marginally exceeding M1, which achieved 66.66 % RSC. Ascorbic acid nevertheless displayed the strongest activity, with an IC_{50} of 0.30 µg/mL, serving as the benchmark for potent antioxidant effects. Taken together, these findings indicate that both M1 and M2 exhibited notable antioxidant properties, with M2 being more effective than M1 and approaching the efficacy of ascorbic acid at higher concentrations, making it a promising candidate for further investigation.

Table 2. Radical scavenging activities and IC_{50} values of the synthesized compounds and standard.

Compound	100µg.mL $^{-1}$	200 µg.mL^{-1}	500 µg.mL^{-1}	800 µg.mL^{-1}	IC_{50}
M1	25	33.33	58.33	66.66	0.46
M2	30.58	40.9	58.88	68.84	0.4
Ascorbic acid	40	45	60	71.66	0.3

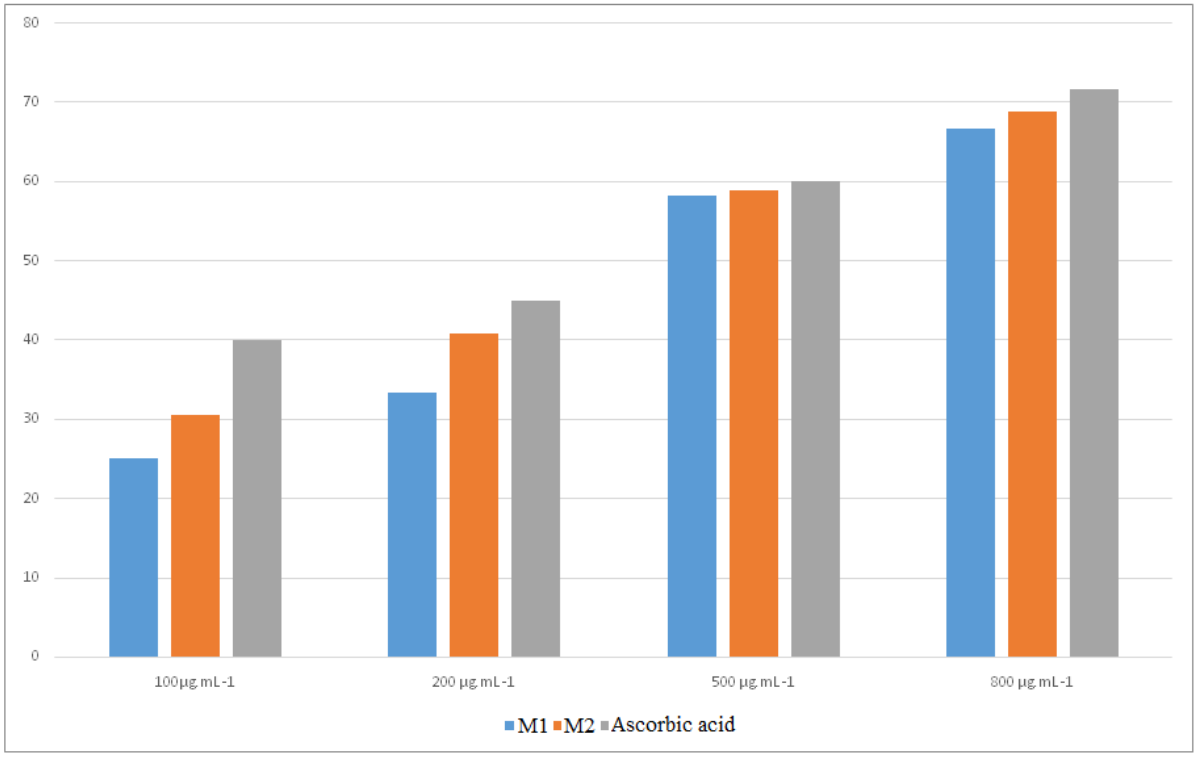

Figure 2. DPPH radical scavenging activity of the synthesized compounds M1 and M2 and the standard.

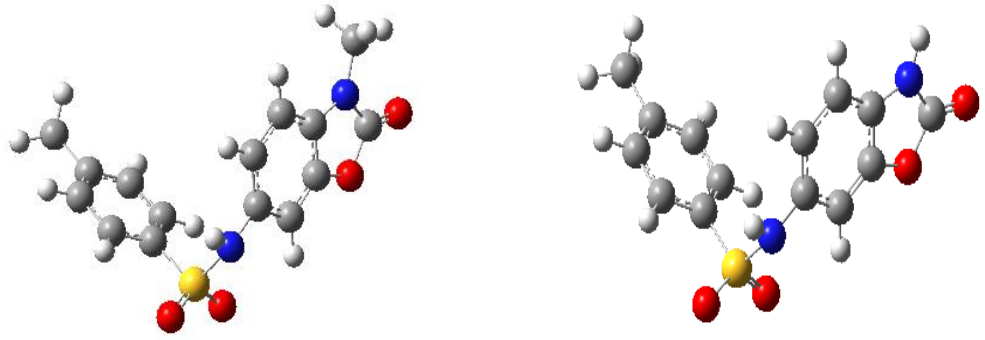

(M1) **(M2)**

Figure 3. Optimized geometries of the synthesized compounds M1 and M2.

Geometry Optimization

Geometry optimization of compounds M1 and M2 was carried out using the DFT method at the B3LYP/6-31+G(d,p) level (**Figure 3**).

Frontier Molecular Orbital Profiles and Global Reactivity Parameters

HOMO and LUMO electron density distributions provide key insights into a compound's chemical stability, highlighting the regions most likely to donate or accept electrons during chemical reactions. These frontier molecular orbitals were evaluated for M1 and M2 based on their optimized geometries (**Figure 4)**.

The energy gap is a key parameter for understanding the electronic properties of a compound, and is generally associated with higher chemical reactivity and lower molecular stability. The HOMO-LUMO profiles, energy gaps, and global reactivity descriptors of M1 and M2 are therefore essential for characterizing their chemical behaviour, and were investigated in this context (**Table 3**).

The results in **Table 3** indicate that compound M2 was more reactive than M1 due to its lower HOMO-LUMO energy gap (4.367eV) and reduced chemical hardness (2.183 eV), which facilitate electron excitation and enhance overall chemical reactivity. This increased reactivity improves its ability to scavenge free radicals and interact efficiently with biological targets. This behaviour is further supported by M2's higher electrophilicity index (ω=4.827eV), highlighting its superior electron-accepting ability, and a larger ΔNmax value (2.102) compared to M1 (1.641), indicating a greater capacity to accommodate and stabilize incoming electron density. M2's higher reactivity explains its stronger antioxidant and antibacterial performance. Moreover, this electronic feature accounts for its longer experimental maximum absorption wavelength (λmax) of 360 nm vs 300 nm for M1, as compounds with smaller energy gaps generally absorb at longer wavelengths.

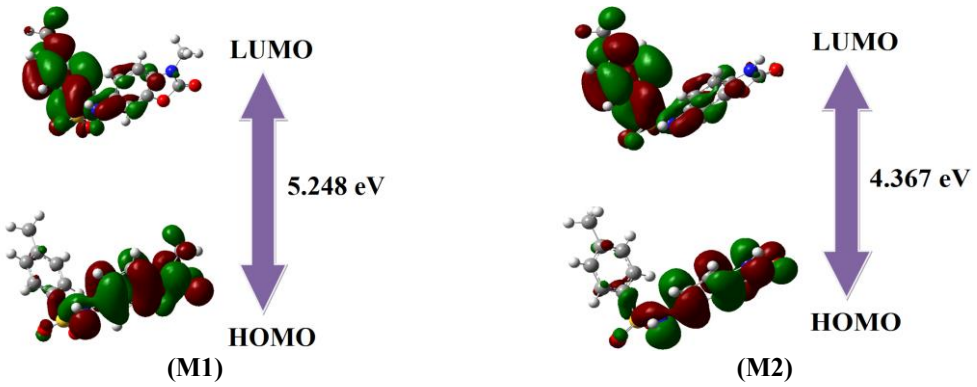

Figure 4. HOMO and LUMO of optimized M1 and M2 structures.

Table 3. Global reactivity descriptors calculated for the synthesized compounds M1 and M2 (in eV).

Compound	M1	M2
E_{HOMO}	-6.930	-6.775
E_{LUMO}	-1.678	-2.408
I	6.930	6.775
A	1.678	2.408
E_{gap}	5.248	4.367
χ	4.304	4.590
μ	-4.305	-4.590
η	2.623	2.183
S	0.381	0.458
ω	3.529	4.827
N	0.233	0.207
ΔN_{max}	1.641	2.102

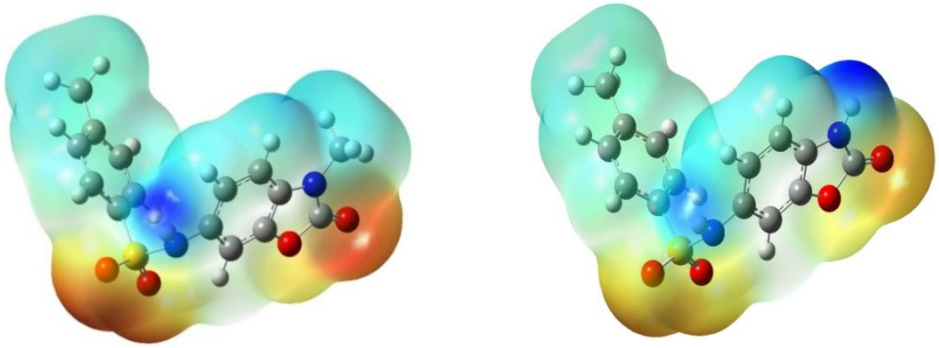

(M1) **(M2)**

Figure 5. MESP distribution of the synthesized compounds M1 and M2.

Molecular Electrostatic Potential

Electrostatic potential maps (MEP) provide essential information on electron density distribution, electropositive and electronegative sites, and potential hydrogen bonding interactions [61]. The molecular electrostatic potential (MESP) surfaces for compounds M1 and M2 were predicted from their optimized geometries (**Figure 5**). The colour-coded molecular electrostatic potential (MESP) surfaces illustrate charge distribution across the molecules. Blue regions, representing high positive electrostatic potential, correspond to electron-deficient zones such as hydrogen atoms or electrophilic sites. In contrast, red regions with low negative potential indicate electron-rich nucleophilic sites, typically around oxygen and sulfur atoms. For both M1 and M2, oxygen and sulfur atoms were enveloped in negative potential, underscoring their electron-rich character. Hydrogen atoms on alkyl/aromatic rings, as well as those in sulfonamide and benzoxazolinone NH groups, resided in positive potential areas. These charge variations modulate interactions with bacterial cell structures, with electron-rich and electron-deficient regions facilitating binding to targets and enhancing antibacterial efficacy.

Fukui Functions

Fukui functions describe electron density distribution within a molecule, providing insights into atoms most likely to donate or accept electrons [62, 63]. These descriptors are essential for identifying sites susceptible to electrophilic or nucleophilic attack. The Fukui function is defined by the following formulations:

For nucleophilic attack $f^{-}k = [qk(N+1) - qk(N)]$

For electrophilic attack $f^{+}k = [qk(N) - qk(N-1)]$

For radical attack $f^{0}k = [qk(N+1) - qk(N-1)]$

Where q(N), q(N+1), and q(N-1) are the electronic populations of the atom k in neutral, cationic and anionic systems respectively [64]. The responsive zones on M1 and M2 were predicted via Gaussian 16 by applying the previous method and UCA Fukui (**Table 4**).

Table 4. Fukui indices (f^+, f^-, f^0) for each atom in the synthesized compounds M1 and M2.

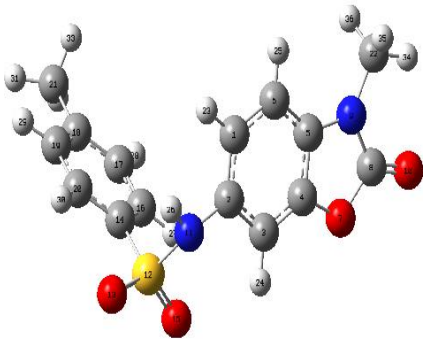

M1

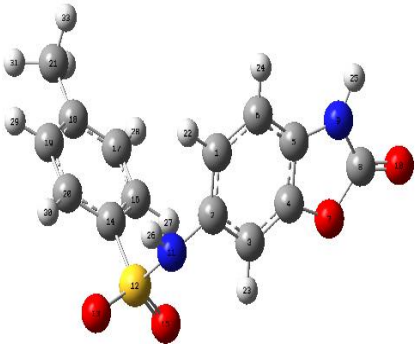

M2

Atom	*f+*	*f-*	*f0*	Atom	*f+*	*f-*	*f0*
1 C	-0,003604	0,031745	0,028836	**1 C**	0.086468	0.24689	0.333358
2 C	-0,004527	0,028264	0,023737	**2 C**	-0.0576849	0.347607	0.067006
3 C	0,025981	0,035394	0,061375	**3 C**	-0.0473175	0.097447	0.050158
4 C	0,008101	0,028294	0,0364	**4 C**	0.031214	-0.249015	-0.217801
5 C	0,035485	0,038051	0,073536	**5 C**	-0.04739	-1.131018	-1.178408
6 C	-0,022088	0,033218	0,055296	**6 C**	0.018801	0.100708	0.119509
7 O	0,0137558	0,032098	0,045856	**7 O**	-0.012148	0.525112	-0.50025
8 C	0,025862	0,044156	0,070018	**8 C**	0.1117162	-0.720297	-0.603099
9 N	-0,007325	0,029807	0,022482	**9 N**	-0.993074	0.732803	0.729729
10 O	0,042917	0,097531	0,140448	**10 O**	0.07229	0.497955	0.570245
11 N	0,013203	0,052546	0,065738	**11 N**	0.008516	0.936535	0.945051
12 S	0,063383	0,008086	0,071469	**12 S**	0.124056	0.182362	0.306418
13 O	0,047103	0,041879	0,088982	**13 O**	0.102802	0.496347	0.599149
14 C	0,024005	-0,009002	0,015003	**14 C**	0.089741	-0.043627	0.046114
15 O	0,038519	0,024515	0,063011	**15 O**	0.083677	0.494385	0.578062
16 C	0,024558	-0,006749	0,017809	**16 C**	0.034697	0.075999	-0.110696
17 C	0,010689	0,009099	0,019788	**17 C**	0.060652	0.13945	0.200102
18 C	0,030469	0,003433	0,033902	**18 C**	0.025943	-0.07676	-0.050817
19 C	0,011168	0,007376	0,018544	**19 C**	0.032557	0.099868	0.132425
20 C	0,023953	0,005942	0,029895	**20 C**	-0.122459	0.106683	-0.015786
21 C	-0,012126	-0,00571	-0,017836	**21 C**	0.102101	0.372828	0.474929
22 C	-0,013638	-0,028651	-0,042289				

Table 4 presents a detailed analysis of the Fukui functions (f^+, f^-, f^0) for compounds M1 and M2. In M1, atom 12 (S) exhibited the highest f^+ value (0.063383), indicating the most electrophilic site. Oxygen atoms 10, 12, and 13 also showed notable f^+ values (0.042917, 0.038519, and 0.047103), identifying additional electrophilic regions. For nucleophilic reactivity (f^-), atom 10 (O) displayed the highest value (0.097531), highlighting its dual reactivity, while atoms 5 (C) and 11 (N) acted as secondary nucleophilic sites. In terms of radical interactions (f^0), atom 10 (O) again demonstrated the highest value (0.140448), followed by atoms 13 (O) and 5 (C) (0.088982 and 0.073536, respectively). In M2, atom 12 (S) was the most electrophilic site (f^+ = 0.124056), with oxygen atoms 10, 13, and 15 contributing significantly (f^+ = 0.07229, 0.102802, 0.083677). For nucleophilic reactivity, atom 11 (N) showed the highest f^- value (0.936535), followed by atoms 9(N) and 7(O) (0.732803 and 0.525112). For radical reactivity, atom 11(N) was most reactive (f^0= 0.945051), with atoms 9(N) and 13(O) showing notable contributions (0.729729 and 0.599149). These reactive sites correlated with the compounds' ability to scavenge free radicals, explaining the observed in vitro antioxidant activity (%RSC and IC_{50} values).

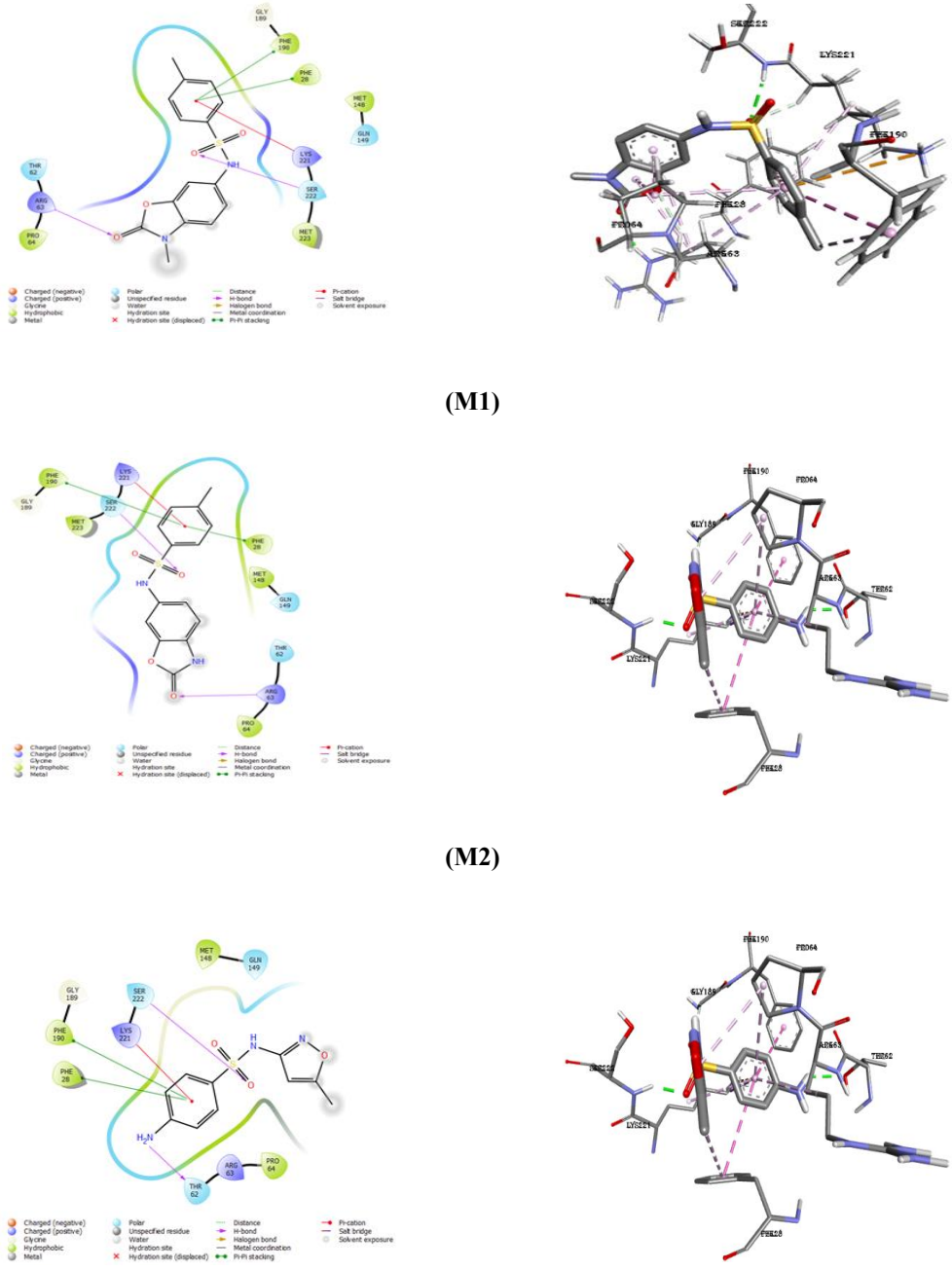

(M1)

(M2)

Co-crystallized ligand

Figure 6. 2D and 3D representations of molecular docking of the synthesized compounds M1 and M2, and sulfamethoxazole into the active site of dihydropteroate synthase (PDB ID: 3TZF).

Molecular Docking

Dihydropteroate synthase (DHPS) represents a key antibacterial target, given its critical role in the bacterial folate biosynthesis pathway. Inhibiting DHPS remains a proven strategy in antibacterial drug development [65]. Molecular docking simulations assessed the binding affinity and interactions of compounds M1 and M2, and the co-crystallized ligand sulfamethoxazole with DHPS (**Figure 6)**. Molecular docking results showed that M2 had the strongest binding affinity to DHPS, with a docking score of -6.974 kcal/mol, surpassing M1 (-6.573 kcal/mol) and the co-crystallized ligand sulfamethoxazole (-6.854 kcal/mol) (Table 5). This superior affinity suggests this compound's enhanced potential for antibacterial activity. Both M1 and M2 formed hydrogen bonds with residues ARG-63 and SER-222, while sulfamethoxazole interacted with THR-62 and SER-222. M1 engaged hydrophobic interactions with MET-223, GLY-189, MET-148, and THR-62, whereas M2 formed a wider array, including MET-

223, GLY-189, MET-148, THR-62, PRO-64, GLN-149, LYS-221, PHE-28, and PHE-190, stabilizing its binding and likely boosting efficacy. These two compounds demonstrated similar binding modes to the crystallized ligand sulfamethoxazole, particularly in the hydrogen bond observed with residue SER-222, and both M1 and M2 shared some hydrophobic interactions with sulfamethoxazole. These results underscore the potential of M1 and M2 as promising candidates for antibacterial activity, given their comparable binding interactions with the co-crystallized ligand. By re-docking of the co-crystallized ligand (sulfamethoxazole), the docking process was validated with an RMSD of less than 1 Å **(Figure 7**).

Drug-likeness Prediction

Examination of drug-likeness and pharmacokinetic properties is essential to evaluate the potential of M1 and M2 as drug candidates. Key physicochemical parameters including molecular weight, number of hydrogen bond acceptors (nHA) and donors (nHD), total polar surface area (TPSA), lipophilicity (LogP), and solubility (LogS) were assessed using SwissADME (**Table 6**).

Table 5. Docking results: affinity scores and interacting residues for the synthesized compounds M1 and M2, and the co-crystallized ligand sulfamethoxazole against DHPS.

		Residual Interactions	
Compound	**Affinity score (Kcal/mol)**	**Hydrogen Bonds**	**Hydrophobic: Pi cation / Pi anion/ Pi Alkyle interaction/ Van der Waals**
M1	-6,573	ARG-63, SER-222	MET-223 GLY-189 MET-148 THR-62
M2	-6,974	ARG-63, SER-222	MET-223 GLY-189 MET-148 THR-62 PRO-64 GLN-149 LYS-221 PHE-28 PHE-190
Sulfamethoxazole (co-crystallized)	-6,854	THR-62 SER-222	PRO-64 PHE-28 ARG-63, MET-148 PHE-190 LYS-221 GLY-189 GLN-149

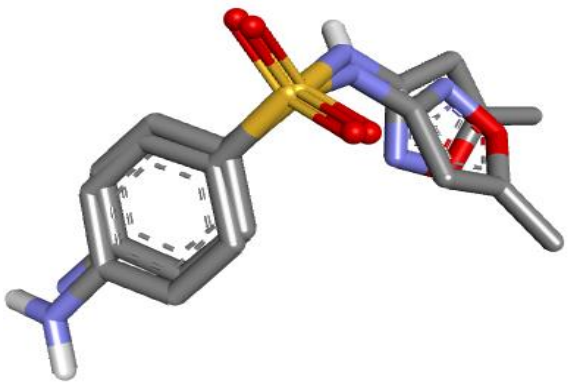

Figure 7. Re-docking of the co-crystallized ligand sulfamethoxazole into the active site of Dihydropteroate Synthase (DHPS).

Table 6. Drug-likeness predictions for synthesized compounds M1 and M2.

Descriptor	M1	M2
Ligands	$C_{14}H_{12}N_2O_4S$	$C_{15}H_{14}N_2O_4S$
Mol.Wt.(g/mol)	304.32	318.35
NRB	3	3
NHA	4	4
NHD	2	1
TPSA(A°²)	100.55	89.69
LogP(cLogP)	2.02	2.12
Log *S*	-3.34	-3.51
violation	0	0
Bioavailability Score	0.55	0.55

Physicochemical Properties:

To assess the drug-likeness and oral bioavailability of compounds M1 and M2, their physicochemical properties were evaluated against Lipinski's Rule of Five. Both compounds satisfied all criteria: their molecular weights of 304.32 g/mol (M1) and 318.35 g/mol (M2) were well below 500 g/mol; M1 had 2 hydrogen bond donors (HBD) and 4 acceptors (HBA), while M2 had 1 HBD and 4 HBA (both ≤5 HBD and ≤10 HBA); logP values of -2.02 (M1) and -2.12 (M2) were under 5. Each featured 3 rotatable bonds, enhancing flexibility. Their topological polar surface areas (TPSA) were 100.55 Å² for M1 and 89.69 Å² for M2, both below the 140 Å² threshold associated with good intestinal absorption. The moderate logP values reflect a favourable balance between lipophilicity for membrane permeability and hydrophilicity for solubility, positioning M1 and M2 as viable oral drug candidates. Under physiological conditions, their aqueous solubility (LogS) values of −3.34 (M1) and −3.51 (M2) indicated acceptable solubility, while a bioavailability score of 0.55 suggested strong potential for oral administration. Overall, these properties confirmed that M1 and M2 were drug-like compounds with promising pharmacokinetic profiles.

Pharmacokinetic Properties

The pharmacokinetic profiles of compounds M1 and M2 were evaluated for key parameters including gastrointestinal (GI) absorption, blood-brain barrier (BBB) permeability, skin permeability (log Kp), and interactions with efflux transporters and metabolic enzymes (**Table 7**). Both compounds exhibited high GI absorption, supporting their potential for oral administration, but neither was predicted to cross the BBB, which may minimize central nervous system side effects. Their log Kp values (-6.72 for M1 and -6.67 for M2) indicated comparable low skin permeability. M2 was projected to inhibit CYP2C19, a cytochrome P450 enzyme involved in drug metabolism, while M1 showed no such inhibition across isoforms. Neither compound was a P-glycoprotein (P-gp) substrate, reducing risks of efflux-mediated drug resistance. These attributes highlight favourable pharmacokinetics suited for systemic applications.

Table 7. Predicted ADME descriptors of the synthesized compounds M1 and M2.

Compound		M1	M2
Skin Permeation Value (log Kp) cm/s		- 6.72	- 6.67
GI Absorption		High	High
BBB Permeability		No	No
Inhibitor Interaction	**P-gp Substrate**	No	No
	CYP1 A2I	No	No
	CYP2 C19	No	No
	CYP2 C9	No	Yes
	CYP2 D6	No	No
	CYP3 A4	No	No

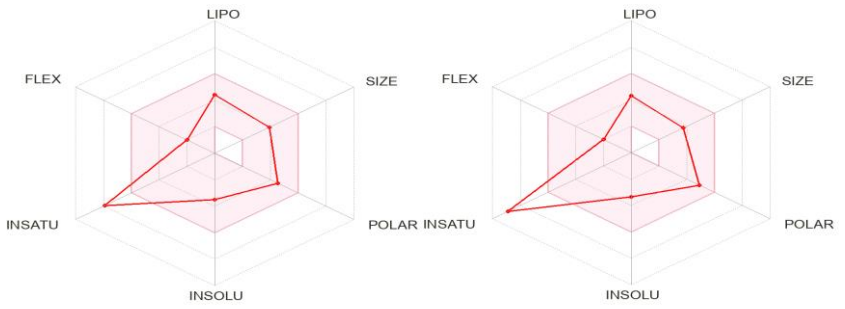

(M1) **(M2)**

Figure 8. SwissADME bioavailability radar plots for compounds M1 and M2.

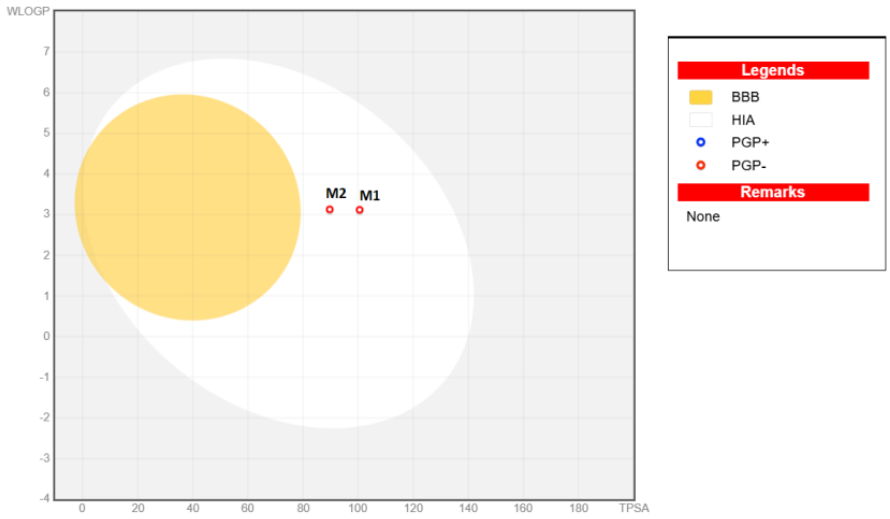

Figure 9. BOILED-Egg plot for compounds M1 and M2, indicating gastrointestinal absorption and blood-brain barrier penetration.

Table 8. Toxicity predictions of the synthesized compounds M1 and M2.

Compound	LD_{50} (mg/kg)	Toxicity Class	Organ Toxicity				
			Hepatotoxicity	Carcinogenicity	Immunotoxicity	Mutagenicity	Cytotoxicity
M1	1700	4	Active	Inactive	Inactive	Inactive	Inactive
M2	1310	4	Active	Inactive	Inactive	Inactive	Inactive

Radar plots of bioavailability (**Figure 8**) with descriptors of lipophilicity (LIPO), size (SIZE), polarity (POLAR), insolubility (INSOLU), saturation (INSATU), and flexibility (FLEX), confirmed optimal oral bioavailability profiles for M1 and M2, as their properties fell within ideal ranges: -0.7 < XLOGP3 < 5.0, 150 < MW < 500 g/mol, 20 < TPSA < 130 Å², -6 < LogS < 0.5, 0.25 < fractionCsp3 < 1, and (0 < number of rotatable bonds < 9). These results underscore the potential of M1 and M2 for effective oral absorption and bioavailability.

The BOILED-Egg plot (**Figure 9**) graphically depicts the potential for passive GI absorption and BBB penetration of M1 and M2. Both compounds fell within the white elliptical region, indicating a high likelihood of human intestinal absorption (HIA), while lying outside the yellow zone, signifying limited BBB penetration. This is a desirable trait for non-CNS drugs to minimize neurological side effects. Their positioning outside red circles confirms they are not P-glycoprotein (P-gp) substrates, reducing the risk of active

efflux and supporting better bioavailability without resistance concerns.

Toxicity Prediction

The toxicity profiles of compounds M1 and M2 (**Table 10**) offer key safety insights. Their LD50 values of 1700 mg/kg for M1 and 1310 mg/kg for M2 classified both in toxicity class 4, denoting low acute toxicity risk with moderate safety margins, though M2 showed slightly higher toxicity. Both were predicted to cause hepatotoxicity, warranting experimental validation for potential liver effects. Positively, neither exhibited carcinogenicity, mutagenicity, immunotoxicity, or cytotoxicity, supporting a favourable long-term safety outlook. While encouraging, M2's hepatotoxicity and narrower margin call for dose optimization. Overall, M1 and M2 hold promise for development, pending liver safety studies.

CONCLUSION

This study introduced an environmentally friendly, ultrasound-assisted synthesis method for two sulfonamide derivatives of 2(3H)-benzoxazolone, M1 and M2, with shorter reaction times. For the first time, their in vitro antimicrobial and antioxidant activities were evaluated, revealing significant biological potential that positions them as candidates for antibacterial and antioxidant applications. Preliminary antioxidant activity was assessed via the DPPH assay, yielding IC_{50} values that demonstrated competitive potential against ascorbic acid (IC_{50} = 0.30 µg/mL), with M2 (0.40 µg/mL) outperforming M1 (0.46 µg/mL). Antimicrobial screening against Gram-positive and Gram-negative pathogens identified M2 as the superior agent, showing dose-dependent inhibition zones comparable or superior to gentamicin, particularly against *Bacillus cereus* and *Salmonella Typhi*. DFT calculations at B3LYP/6-31G+(d,p) exhibited M2's higher reactivity (smaller HOMO-LUMO gap, higher electrophilicity), correlating with its biological efficacy, while Fukui functions and MESP maps pinpointed reactive sites. Molecular docking against DHPS (PDB: 3TZF) confirmed M2's top binding affinity (-6.974 kcal/mol). SwissADME analysis affirmed drug-likeness (Lipinski compliance), high GI absorption, no BBB penetration, and bioavailability score of 0.55; toxicity was predicted as low acute risk (class 4) but hepatotoxicity was flagged for validation. Future efforts should prioritize efficacy-safety optimization for therapeutic advancement.

ACKNOWLEDGEMENTS

The authors gratefully acknowledge the resources provided by the Catholic University of Louvain in Brussels, Mohamed Cherif Messaadia University of Souk Ahras, and the Platform of Physico-Chemical Analysis (PTAPC-CRAPC) in Laghouat for the spectroscopic analysis.

REFERENCES

1. Park, J. J., Park, H., Na, S. H., Seo, Y. B. & Lee, J. (2024) Trends of antimicrobial susceptibilities and multidrug-resistant colonization rate in patients transferred from long-term care facilities during 2017–2022: a cross-sectional study. *BMC Infectious Diseases*, **24(1)**, 235.

2. Parra, G., Lautenbach, E., Mosepele, M., Mannathoko, N., Gross, R., Call, D. R. & Styczynski, A. (2025) Colonization with antibiotic resistant bacteria in communities and hospitals across six countries, including Bangladesh, Botswana, Chile, Guatemala, India, and Kenya. *Scientific Reports*, **15(1)**, 21275.

3. Aldarhami, A., Elrggal, M., Alzaylaee, R. A., Almushri, K. K., Alamri, M. A., Imam, M. & Bazaid, A. S. (2025) Patterns of resistance among critically ill patients at a Territory Hospital, Saudi Arabia: A retrospective cohort study. *Medicine*, **104(41)**, e45159.

4. Dagah, O. M. A., Silaa, B. B., Zhu, M., Pan, Q., Qi, L., Liu, X. & Yudas, A. F. (2024) Exploring Immune Redox Modulation in Bacterial Infections: Insights into Thioredoxin-Mediated Interactions and Implications for Understanding Host-Pathogen Dynamics. *Antioxidants (Basel)*, **13(5)**.

5. Di Martino, R., Picot, A. & Mitri, S. (2024) Oxidative stress changes interactions between 2 bacterial species from competitive to facilitative. *PLoS Biology*, **22(2)**, e3002482.

6. Qi, W., Jonker, M. J., Teichmann, L., Wortel, M. & Ter Kuile, B. H. (2023) The influence of oxygen and oxidative stress on de novo acquisition of antibiotic resistance in E. coli and Lactobacillus lactis. *BMC Microbiology*, **23(1)**, 279.

7. Sahoo, D. K., Wong, D., Patani, A., Paital, B., Yadav, V. K., Patel, A. & Jergens, A. E. (2024) Exploring the role of antioxidants in sepsis-associated oxidative stress: a comprehensive review. *Frontiers in Cellular and Infection Microbiology*, **14**, 1348713.

8. Šiugždaitė, J., Lelešius, R., Grybaitė, B., Vaickelionienė, R. & Mickevičius, V. (2024) Synthesis and biological studies of new 2-benzoxazolinone derivatives as antibacterial agents. *Applied Sciences*, **14(11)**, 4783.

9. Prasher, P., Mall, T. and Sharma, M. (2023) Synthesis and biological profile of benzoxazolone derivatives. *Archiv der Pharmazie*, **356(9)**, 2300245.

10. Nessaibia, H., Khaoua, O., Guenadil, F., Messaoudi, A. & Benbellat, N. (2025) Green Synthesis, Drug Design, In Vitro Antibacterial and Antioxidant Activities, DFT Analysis, and MD Analyses of Two N-Naphthoyl Benzoxazolone and Benzothiazolone Derivatives. *ChemistrySelect*, **10(20)**, e00890.

11. Prashanth, G. K., Rao, S., Lalithamba, H. S., Rashmi, K. V., Bhagya, N. P., Ghosh, M. K. & Darekar, N. R. (2025) Benzoxazoles: Diverse Biological Activities and Therapeutic Potential. In *Five Membered Bioactive N and O-Heterocycles: Models and Medical Applications, IGI Global Scientific Publishing*, 317–342.

12. Koçak Aslan, E., Sağlık, B. N., Özkay, Y. & Palaska, E. (2023) Synthesis and Biological Evaluation of Benzoxazolone− Thiosemicarbazide, 1, 2, 4-Triazole, 1, 3, 4-Thiadiazole Derivatives as Cholinesterase Inhibitors. *ChemistrySelect*, **8(35)**, e202302069.

13. Zhang, N., Zeng, W., Zhou, Q., Sun, Z., Meng, K., Qin, Y. & Xue, W. (2024) Design, synthesis, antibacterial and antiviral evaluation of chalcone derivatives containing benzoxazole. *Arabian Journal of Chemistry*, **17(1)**, 105368.

14. Nessaibia, H., Guenadil, F. & Khaoua, O. (2025) Synthesis, in vitro antibacterial and antioxidant evaluation, DFT calculation, molecular docking, and ADMET studies of novel N-Acyl-6-chloro-2 (3H)-benzoxazolone derivatives. *Journal of Molecular Structure*, **1322**, 140308.

15. Kovács, F., Huliák, I., Árva, H., Kocsis, M., Kiricsi, M. & Frank, É. (2025) Aromatic scaffold-integrated hybrids of estradiol and benzoxazol-2-ones: synthesis and in vitro anticancer activity of N-substituted regioisomeric pairs. *RSC Advances*, **15(29)**, 23954–23965.

16. Haskologlu, I. C., Erdag, E., Sehirli, A. O., Uludag, O. & Abacioglu, N. (2024) Exploring the Therapeutic Potential of Benzoxazolone Derivatives on the Circadian Clock: An In Silico and Hypothetical Approach. *Chronobiol. Med*., **6(2)**.

17. Ge, R., Song, J., Cao, Z., Ban, S., Tang, L. & Li, Q. S. (2024) Discovery of 6-Acylamino/Sulfonamido Benzoxazolone with IL-6 Inhibitory Activity as Promising Therapeutic Agents for Ulcerative Colitis. *Chemistry & Biodiversity*, **21(5)**, e202400031.

18. Majhi, S., Manickam, S. & Cravotto, G. (2025) Ultrasound-assisted green synthesis of functionalised xanthene derivatives: Advancing sustainable sonochemical strategies. *Ultrasonics Sonochemistry*, **107367**.

19. Haseli, K., Esmkhani, M. & Javanshir, S. (2025) Ultrasound-assisted green synthesis of 1, 4-disubstituted 1, 2, 3-triazoles using natural polymer supports. *Scientific Reports*, **15(1)**, 28624.

20. Borah, B. & Chowhan, L. R. (2022) Ultrasound-assisted transition-metal-free catalysis: a sustainable route towards the synthesis of bioactive heterocycles. *RSC Advances*, **12(22)**, 14022–14051.

21. Zelelew, D., Endale, M., Melaku, Y., Geremew, T., Eswaramoorthy, R., Tufa, L. T. & Lee, J. (2023) Ultrasonic-Assisted Synthesis of Heterocyclic Curcumin Analogs as Antidiabetic, Antibacterial, and Antioxidant Agents Combined with in vitro and in silico Studies. *Advances and Applications in Bioinformatics and Chemistry*, 61–91.

22. Ibrahim, A. G., Hamodin, A. G., Fouda, A., Eid, A. M. & Elgammal, W. E. (2024) Fabrication and characterization of a new eco-friendly sulfonamide-chitosan derivative with enhanced antimicrobial and selective cytotoxicity properties. *Scientific Reports*, **14(1)**, 10228.

23. Mushtaq, I. & Ahmed, A. (2023) Synthesis of biologically active sulfonamide-based indole analogs: a review. *Future Journal of Pharmaceutical Sciences*, **9(1)**, 46.

24. Hussien, A., Musa, A., El-Din, H. T. N., Helal, A. M., Nagy, Y. I., Ezzat, H. G. & Elsebaie, M. M. (2025) Phenyltriazole-based sulfonamides: novel dual-target agents against MRSA biofilms and resistant pathogens. *RSC Advances*, **15(22)**, 17186–17202.

25. Deshmukh, H. S., Adole, V. A., Mali, S. N. & Jagdale, B. S. (2025) Design, synthesis, biological evaluation, and computational insights of 2-(Aryl) benzo [d] imidazo [2, 1-b] thiazole-7-sulfonamide derivatives as potent antitubercular and antibacterial agents. *BMC Chemistry*, **19(1)**, 126.

26. Vaickelionienė, R., Petrikaitė, V., Vaškevičienė, I., Pavilonis, A. & Mickevičius, V. (2023) Synthesis of novel sulphamethoxazole derivatives and exploration of their anticancer and antimicrobial properties. *PLoS One*, **18(3)**, e0283289.

27. Kumar, M., Ramasamy, K., Mani, V., Mishra, R. K., Majeed, A. B., De Clercq, E. and Narasimhana, B. (2014) Synthesis, antimicrobial, anticancer, antiviral evaluation, and QSAR studies of 4-(1-aryl-2-oxo-1, 2-dihydro-indol-3-ylideneamino)-N-substituted benzene sulfonamides, *Arabian Journal of Chemistry*, **7(4)**, 396–408.

28. Abbas, H. A. S., Nossier, E. S., El-Manawaty, M. A. & El-Bayaa, M. N. (2024) New sulfonamide-based glycosides incorporated 1, 2, 3-triazole as cytotoxic agents through VEGFR-2 and carbonic anhydrase inhibitory activity. *Scientific Reports*, **14(1)**, 13028.

29. Alkaoud, A. M., Alakhras, A. I., Ibrahim, M. A., Alghamdi, S. K. & Hussein, R. K. (2024) In silico evaluation of a new compound incorporating 4 (3H)-quinazolinone and sulfonamide as a potential inhibitor of a human carbonic anhydrase. *BMC Chemistry*, **18(1)**, 45.

30. Faydali, N., Erol, M., Temiz Arpaci, O., Kuyucuklu, G. & Semih Salan, A. (2025) Novel sulfonylamido benzoxazole derivatives: synthesis, characterisation, molecular docking, DFT, and antimicrobial activity investigations. *Chemistry & Biodiversity*, **22(2)**, e202402127.

31. Erol, M., Acar-halıcı, C., Kuyucuklu, G., Salan, A. S. & Temiz-arpacı, Ö. (2024) New Sulfonamido-Benzoxazole Derivatives as Antimicrobial Agents: Design, Synthesis and Biological Evaluation. *Journal of Faculty of Pharmacy of Ankara University*, **48(1)**, 150–157.

32. Deshmukh, H. S., Adole, V. A., Mali, S. N. & Jagdale, B. S. (2025) Design, synthesis, biological evaluation, and computational insights of 2-(Aryl) benzo [d] imidazo [2, 1-b] thiazole-7-sulfonamide derivatives as potent antitubercular and antibacterial agents. *BMC Chemistry*, **19(1)**, 126.

33. Weyesa, A., Eswaramoorthy, R., Melaku, Y. and Mulugeta, E. (2021) Antibacterial, docking, DFT and ADMET properties evaluation of chalcone-sulfonamide derivatives prepared using ZnO nanoparticle catalysis. *Advances and Applications in Bioinformatics and Chemistry,* 133–144.

34. Carvalho, R. S., Carollo, C. A., De Magalhães, J. C., Palumbo, J. M. C., Boaretto, A. G., e Sá, I. N. and Ferreira, J. M. S. (2018) Antibacterial and antifungal activities of phenolic compound-enriched ethyl acetate fraction from Cochlospermum regium (mart. Et. Schr.) Pilger roots: Mechanisms of action and synergism with tannin and gallic acid., *South African Journal of Botany*, **114**, 181–187.

35. O.Khaoua, N., Benbellat, S., Zeroual, S., Mouffouk, S., Golhen, A., Gouasmia, H. and Chermette, H. (2023) Combined experimental, computational studies (synthesis, crystal structural, DFT calculations, spectral analysis) and biological evaluation of the new homonuclear complex Di-μ-benzoato-bis [benzoatodipyridine-cobalt (II)], *Journal of Molecular Structure*, **1273**, 134331.

36. Frisch, M. J., Trucks, G. W., Schlegel, H. B., Scuseria, G. E., Robb, M. A., Cheeseman, J. R., Scalmani, G., Barone, V., Petersson, G. A., Nakatsuji, H., Li, X., Caricato, M., Marenich, A. V., Bloino, J., Janesko, B. G., Gomperts, R., Mennucci, B., Hratchian, H. P., Ortiz, J. V., Izmaylov, A. F., Sonnenberg, J. L., Williams-Young, D., Ding, F., Lipparini, F., Egidi, F., Goings, J., Peng, B., Petrone, A., Henderson, T., Ranasinghe, D., Zakrzewski, V. G., Gao, J., Rega, N., Zheng, G., Liang, W., Hada, M., Ehara, M., Toyota, K., Fukuda, R., Hasegawa, J., Ishida, M., Nakajima, T., Honda, Y., Kitao, O., Nakai, H., Vreven, T., Throssell, K., Montgomery Jr., J. A., Peralta, J. E., Ogliaro, F., Bearpark, M. J., Heyd, J. J., Brothers, E. N., Kudin, K. N., Staroverov, V. N., Keith, T. A., Kobayashi, R., Normand, J., Raghavachari, K., Rendell, A. P., Burant, J. C., Iyengar, S. S., Tomasi, J., Cossi, M., Millam, J. M., Klene, M., Adamo, C., Cammi, R., Ochterski, J. W., Martin, R. L., Morokuma, K., Farkas, O.,. Foresman, J. B, Fox, D. J. (2016) Gaussian 16, Revision B.01. *Gaussian Inc., Wallingford (CT)*.

37. Anza, M., Endale, M., Cardona, L., Cortes, D., Eswaramoorthy, R., Zueco, J. and Abarca, B. (2021) Antimicrobial activity, in silico molecular docking, ADMET and DFT analysis of secondary metabolites from roots of three Ethiopian medicinal plants. *Advances and Applications in Bioinformatics and Chemistry*, 117–132.

38. Madhavi Sastry, G., Adzhigirey, M., Day, T., Annabhimoju, R. and Sherman, W. (2013) Protein and ligand preparation: Parameters, protocols, and influence on virtual screening enrichments. *Journal of Computer Aided Molecular Design*, **27**, 221–234.

39. Lipinski, C. A. (2016) Rule of five in 2015 and beyond: target and ligand structural limitations, ligand chemistry structure, and drug discovery project decisions. *Advanced Drug Delivery Reviews*, **101**, 34–41.

40. Nabid, M. R., Rezaei, S. J. T., Ghahremanzadeh, R. and Bazgir, A. (2010) Ultrasound-assisted one-pot, three-component synthesis of 1H-pyrazolo [1, 2-b] phthalazine-5, 10-diones. *Ultrasonics Sonochemistry*, **17(1)**, 159–161.

41. Danjou, P. E., Wallyn, D., Cazier-Dennin, F. and Delattre, F. (2012) Ultrasound-promoted tosylation of oligo (ethylene glycols), *Ultrasonics Sonochemistry*, **19**(6), 1201–1204.

42. Pham, H. T., Nguyen, N. L. T., Duus, F. and Luu, T. X. T. (2015) Ultrasound-accelerated synthesis of asymmetrical thiosulfonate S-esters by base-promoted reaction of sulfonyl chlorides with thiols. *Phosphorus, Sulfur, and Silicon and the Related Elements*, **190(11)**, 1934–1941.

43. Nimbalkar, U. D., Seijas, J. A., Borkute, R., Damale, M. G., Sangshetti, J. N., Sarkar, D. and Nikalje, A. P. G. (2018) Ultrasound assisted synthesis of 4-(benzyloxy)-N-(3-chloro-2-(substitutedphenyl)-4-oxoazetidin-1-yl) benzamide as challenging anti-tubercular scaffold. *Molecules*, **23(8)**, 1945.

44. Cheraiet, Z., Meliani, S., Nessaib, M., Hessainia, S., Boukhari, A., Djahoudi, A. and Regainia, Z. (2019) Scalable synthesis and antibacterial evaluation of 2-(3-(N-(substituted phenyl) sulfamoyl) ureido) benzothiazoles. *Archiv der Pharmazie*, **352(8)**, 1800341.

45. Guenadil, F., Aichaoui, H., Kapanda, C. N., Lambert, D. M., McCurdy, C. R. and Poupaert, J. H. (2011) Design and synthesis of 3-acyl-2(3H)-benzoxazolone and 3-acyl-2(3 H)-benzothiazolone derivatives. *Monatshefte foŘr Chemie-Chemical Monthly*, **142**, 67–80.

46. Yahia, W., Khorief Nacereddine, A., Seddiki, K. and Liacha, M. (2015) Experimental and theoretical investigation of the intramolecular cyclisation of N-(Benzoxazolinon-6-yl) maleimide derivatives. *Revue Roumaine de Chimie*, **60**(9), 853–859.

47. Lespagnol, C. (1955) *Bulletin de la Société de Pharmacie Lille*, **1**, 71–81.

48. Gülkok, Y., Biçer, T., Onurdağ, F. K., Özgen, S., Şahin, M. F. and Doğruer, D. S. (2012) Synthesis of some new urea and thiourea derivatives and evaluation of their antimicrobial activities. *Turkish Journal of Chemistry*, **36(2)**, 279–291.

49. Rayner, C. M. (2007) The Potential of Carbon Dioxide in Synthetic Organic Chemistry. *Organic Process Research & Development*, **11**, 121–132.

50. Adjeroud, Y., Chabane, H. and Liacha, M. (2016) Comparative study of conventional and microwave-assisted synthesis of novel 6-(arylideneamino) benzo[d]oxazol-2(3H)-ones with potential anti-bacterial activity. *Revue Roumaine de Chimie*, **61(2)**, 111–117.

51. Savun-Hekimoğlu, B. (2020) A review on sono-chemistry and its environmental applications. *Acoustics*, **2(4)**, 766–775.

52. Miethchen, R. (1992) Selected applications of sonochemistry in organic chemistry. *Ultrasonics*, **30(3)**, 173–179.

53. Mojtahedi, M. M. and Abaee, M. S. (2011) Ultrasound Applications in Synthetic Organic Chemistry. *Handbook on Applications of Ultrasound*, **739**.

54. Mohamed, M. (2016) Sonochemistry (applications of ultrasound in chemical synthesis and reactions): a review part I. *Al-Azhar Journal of Pharmaceutical Sciences*, **53(1)**, 108–122.

55. Ahmed, M. A. and Mohamed, A. A. (2024) *iScience*, **27**, 108583.

56. Alzahrani, A. Y., Shehab, W. S., Amer, A. H., Assy, M. G., Mouneir, S. M., Abdelaziz, M. & Hamid, A. M. A. (2024) Correction: Design, synthesis, pharmacological evaluation, and in silico studies of the activity of novel spiro pyrrolo [3, 4-d] pyrimidine derivatives. *RSC Advances*, **14(49)**, 36351–36351.

57. Gulcin, İ. & Alwasel, S. H. (2023) DPPH radical scavenging assay. *Processes*, **11(8)**, 2248.

58. Panditharathna, G. M., DewageDona, D. H. D. & Rajapakse, C. S. K. (2025) Comparative analysis of the nutritional, medicinal, and sun protection properties of almond (Prunus dulcis) and tropical almond (Terminalia catappa) nuts. *Food Science and Applied Biotechnology*, **8(2)**, 182–192.

59. Soni, R. (2025) Isolation And Characterization of Novel Bioactive Compounds from Endemic Medicinal Plants of The Western Ghats. *International Journal of Pharmacognosy and Herbal Drug Technology*, 134–146.

60. Chavan, N. D. & Vijayakumar, V. (2024) Synthesis, DFT studies on a series of tunable quinoline derivatives. *RSC Advances*, **14(29)**, 21089–21101.

61. Shalaby, M. A., Fahim, A. M. & Rizk, S. A. (2023) Antioxidant activity of novel nitrogen scaffold with docking investigation and correlation of DFT stimulation. *RSC Advances*, **13(21)**, 14580–14593.

62. Zamora Yates, P. P. & Bieger, K. (2025) Systematic Approach to Negative Fukui Functions: Its Association with Nitro Groups in Aromatic Systems. *International Journal of Molecular Sciences*, **26(1)**, 319.

63. Sigmund, L. M., Assante, M., Johansson, M. J., Norrby, P. O., Jorner, K. & Kabeshov, M. (2025) Computational tools for the prediction of site-and regioselectivity of organic reactions. *Chemical Science*, **16(13)**, 5383–5412.

64. Khaled, K. F. (2010) Studies of iron corrosion inhibition using chemical, electro-chemical and computer simulation techniques. *Electrochimica Acta*, **55(22)**, 6523–6532.

65. Khalaf, H., El-Sayed, A., Sediek, A. & Radwan, M. (2025) Synthesis, molecular docking, ADMET studies and biological evaluation of fused pyrazolopyridopyrimidine derivatives as anti-oxidant and antimicrobial agents. *Scientific Reports*.